SURFACE SCIENCE 40 (1973) 512–530 © North-Holland Publishing Co.

THE GROWTH OF THIN PbO LAYERS ON LEAD FILMS

I. EXPERIMENT

J. M. ELDRIDGE and D. W. DONG

IBM Thomas J. Watson Research Center, Yorktown Heights, New York 10598, U.S.A.

Received 26 December 1972; revised manuscript received 4 June 1973

The growth of ~ 10 to 100 Å thick, orthorhombic PbO layers on lead was investigated by ellipsometry, electron tunneling and X-ray diffraction. Oxides were grown on 2000 to 15000 Å thick, vacuum-deposited lead films, using: oxygen pressures from 10^{-2} to 10^{-3} Torr; temperatures from -90 to $+150$°C; and, times up to several weeks. Apparatus is described for monitoring ellipsometric parameters during oxidation and fabricating Pb–PbO–Pb tunnel junction devices *in situ*. The results indicate that lead recrystallization processes can accelerate the oxidation, so that the rates depend complexly on temperature, lead thickness and microsctructure. The refractive indices provide an indication of the extent of lead recrystallization effects on the oxidation process as well as the accuracy of the oxide thickness determination. X-ray findings indicate that the PbO has the orthorhombic PbO structure, is highly strained while being epitaxially related to the lead, and has a thickness close to that obtained ellipsometrically. Electron tunneling data provide a measure of oxide thickness fluctuations from the average or ellipsometrically-derived values.

1. Introduction

In order to develop solid state technologies utilizing electron tunneling effects, techniques must be developed for precisely forming and analyzing the thin (< 100 Å) dielectric barrier layer. Past works has typically employed oxide barriers, grown thermally in oxygen or plasma ambients[1]) on silicon and vacuum-deposited metal base electrodes. The currents are quite sensitive to the oxide thickness[2,3]) and composition although the latter has not yet been investigated systematically. From extensive results on a variety of metals, the growth and morphology of these ultra-thin oxide films are known to be strongly influenced by several factors including pressure, temperature, impurities, light, stresses, metal orientation and microstructure. Since growing oxide layers frequently develop large fluctuations from their average thicknesses, due to the preferred crystallite growth at certain surface sites[4]), it is not surprising that most tunnel junction studies have been hampered by a lack of experimental reproducibility[5]).

This study was motivated by a desire to explore the potential of Josephson superconductive tunnel junctions for ultra-high performance memory and

logic applications[6]). Since lead is an excellent superconductor, its oxidation and tunneling characteristics were investigated using an experimental system for following oxide growth and fabricating metal–oxide–metal devices with known barrier thicknesses. Remarkably reproducible 20 to 30 Å thick PbO tunnel barriers have been grown on lead using this approach[2]).

In this part of the paper, the apparatus design and operation is outlined. Lead oxidation data are then analyzed to illustrate, using the ellipsometrically-derived optical constants of metal and oxide layers, that the surface topography of the films must be carefully preserved in order to obtain precise oxide thicknesses. The requisite lead microstructural stability will be seen to depend on temperature, lead thickness and morphology, the last being determined by whether sapphire or mica crystals are used as supporting substrates. Effects of oxygen pressure and temperature on the oxidation rate will be presented then, following by X-ray diffraction and tunneling results. A theoretical model for the oxidation behavior of lead is given in the second part of this paper.

2. Experimental procedure

The apparatus consists of a bakeable, ultra-high vacuum system equipped with an ellipsometer and having provisions for depositing metal films through masks to form base and top electrodes for tunnel junctions. The ellipsometer and a sectional view of the reaction chamber are shown in fig. 1. Base pressures of 10^{-10} Torr were reached using U.H.V. pumps, after a 200 °C bakeout. The angle of incidence of the light beam to the substrate was 70.00°. Window strain effects on the polarization of the light were eliminated by joining 1/8 in. thick glass windows to stainless steel bellows mounted on the system via U.H.V. flanges. Window alignment was maintained by loose fitting collars. For pressure differentials up to one atmosphere across the windows and with varying bolt forces on the flanges, the total window corrections on the Polarizer and Analyzer readings were negligible, being $\lesssim 0.1°$ and 0.01°, respectively.

The effect of reflection on the polarization of monochromatic light (here 5461 Å) is determined in ellipsometry. The polarization state is defined by phase and amplitude relationships between the p and s plane wave components of the electric field vector. The p-wave lies in the incident plane, normal to the s-wave. If the incident and reflected beam amplitudes are designated as I and R, respectively, and the phase angle as β, then one can compute[7]) from Δ and ψ the complex refractive index $[n^*_{Pb} = n_{Pb}(1 - i\,\kappa_{Pb})]$ of the *unoxidized* lead, where n_{Pb} is the index, κ_{Pb} is the extinction coefficient, and $i = \sqrt{(-1)}$, and:

$$\Delta \equiv (\beta_p - \beta_s)_{\text{reflected}} - (\beta_p - \beta_s)_{\text{incident}}, \tag{1}$$

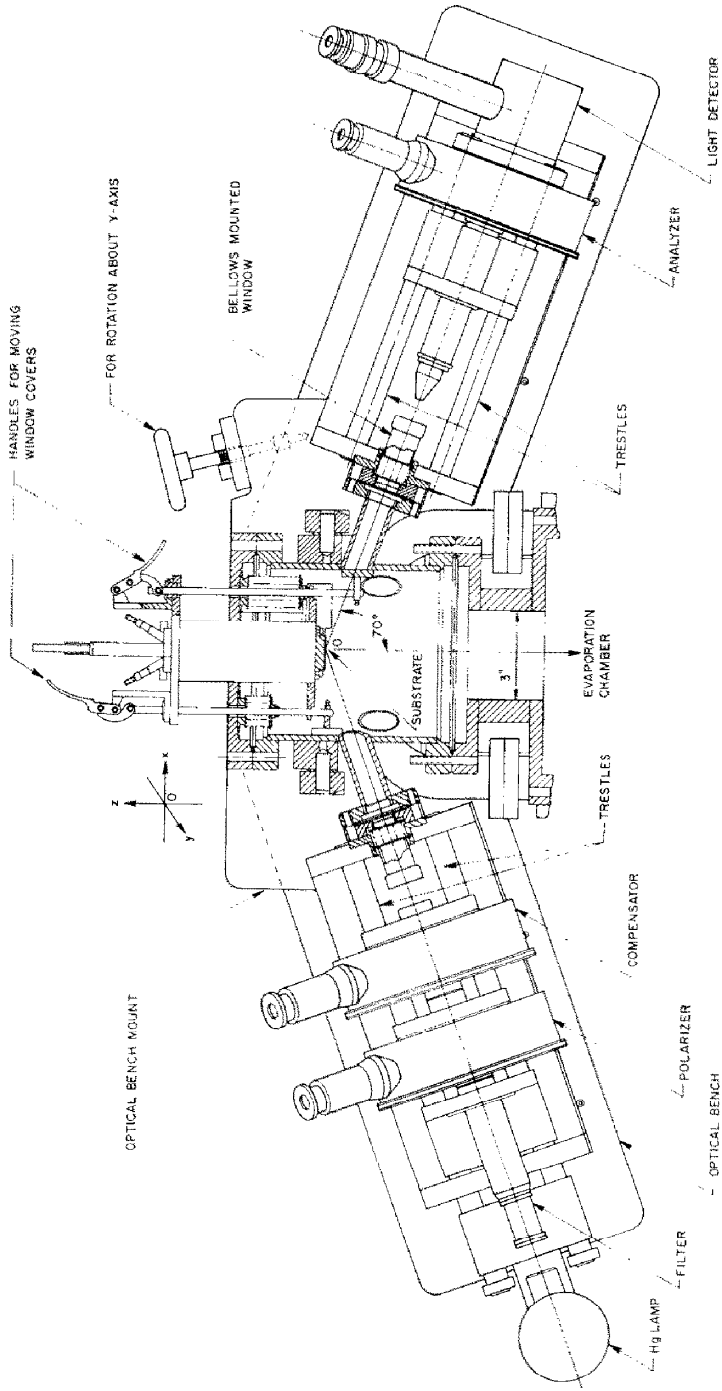

Fig. 1. Sketch of the front of the apparatus, showing cutaway view of 6 in. dia. reaction chamber, location of ellipsometer components, and coordinate system.

$$\psi \equiv \arctan \frac{R_p}{R_s} \cdot \frac{I_s}{I_p}. \tag{2}$$

From Δ and ψ changes on adding O_2, the thickness (X) and either n or κ of the oxide can be determined; frequently n is known or κ is assumed to have a value of zero.

In order to optimally align the ellipsometer relative to the coordinate axis centered at point O, its components (Rudolph Research, Inc.) were mounted on trestles bolted to an optically flat, aluminum plate (1 in. thick × 8 in. wide × 44 in. span). This plate functioned as an optical bench, and was connected by a steel pin to a second plate; large springs kept the plates in contact via spacers while permitting rotation about the y-axis. The second plate was pivoted on pins on the reaction chamber. Thus, the ellipsometer could be rotated about the x- and y-axes by turning screws and translated by the use of x-, y-, and z-slides. (See fig. 2.)

Chem-mechanically polished (0001)-oriented, 1 in. dia. sapphire and cleaved mica crystals were used to support the lead films. After degreasing in trichlorethylene and rinsing in acetone, Cr–Au metallic contact lands (shaded areas in fig. 3) were deposited in another vacuum system. The substrate was mounted with the lands facing the lead source, unto the bottom of a cylindrical copper block. Separate lead film resistance measurements were made to calibrate the film temperature; from the known Pb resistivity temperature dependence, the film and block temperature were found to be within 2° of each other from −100 °C to +150 °C.

The base electrode and resistivity lines and the sampling area for the light beam (fig. 3) were deposited through a 0.003 in. thick Mo mask, at the desired oxidation temperature (in the −90 °C to +150 °C range). A deposition rate of 25 Å/sec was used with a maximum background pressure of 10^{-7} Torr to make 2000 to 15000 Å thick layers. After deposition, the pressure recovered to the $\sim 10^{-9}$ Torr range within a few minutes and the film was vacuum annealed for an hour or two. High purity oxygen was introduced to the desired pressure (from 10^{-2} to 10^{+3} Torr) and oxidation was followed ellipsometrically for times from a few minutes up to several weeks. Counter-electrodes were vacuum deposited at room temperature through a second mask, and the Josephson junction characteristics were measured elsewhere.

3. Results and discussion

3.1. Interpretation of ellipsometric data

Provided the temperatures were not too high, the lead films exhibited reproducible, stable refractive index values, which varied somewhat with

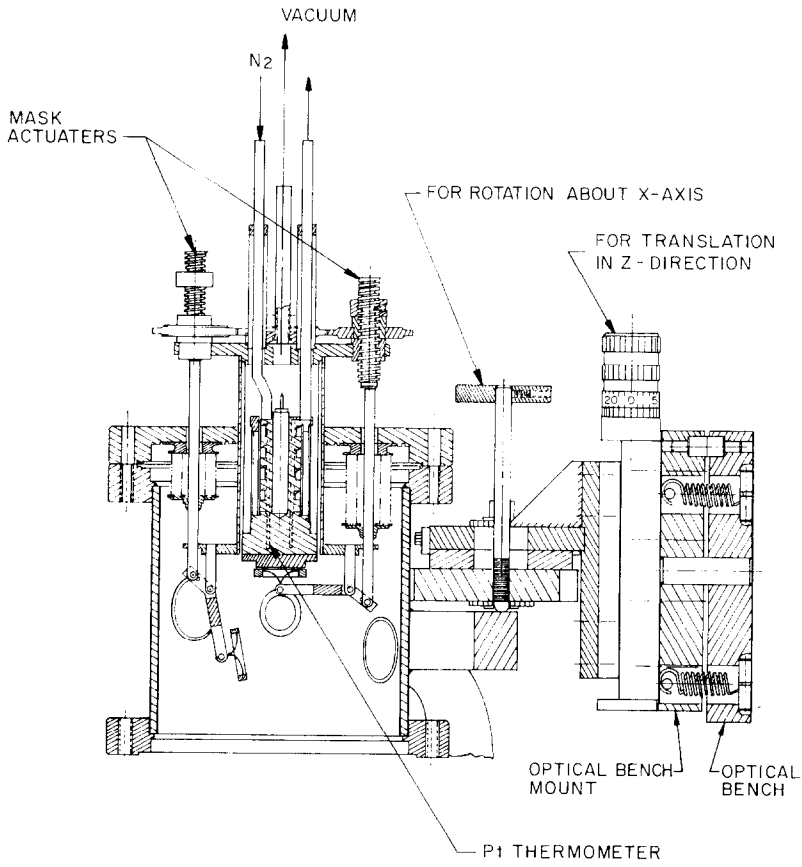

Fig. 2. Sectional view of the side of the chamber and ellipsometer mount, illustrating masking and alignment features.

temperature and substrate material. X-ray[10]) and electron microscope analyses indicated that the films had a nearly perfect (111) preferred orientation and a grain diameter of $\sim$2000 Å for a film thickness of $\sim$3000 Å when deposited on sapphire; the thinner lead layers had smaller grain sizes, as expected. With mica substrates, the films were essentially single crystalline with the (111) plane again exposed.

In order to obtain maximum accuracy, X and n_{PbO} were computed directly from the Δ, ψ data sets assuming various values of κ_{PbO}. However, it is easier to see the various inter-dependencies of X, n_{PbO} and κ_{PbO} on the Δ, ψ parameters when the relationships are displayed graphically. Thus, the family of curves shown in fig. 4 were calculated assuming $\kappa_{PbO}=0$. The Δ, ψ points from two runs were included to show that $n_{PbO}\simeq 2.8$. This is reasonable for stoichiometric, orthorhombic PbO, which has n and κ values of 2.7

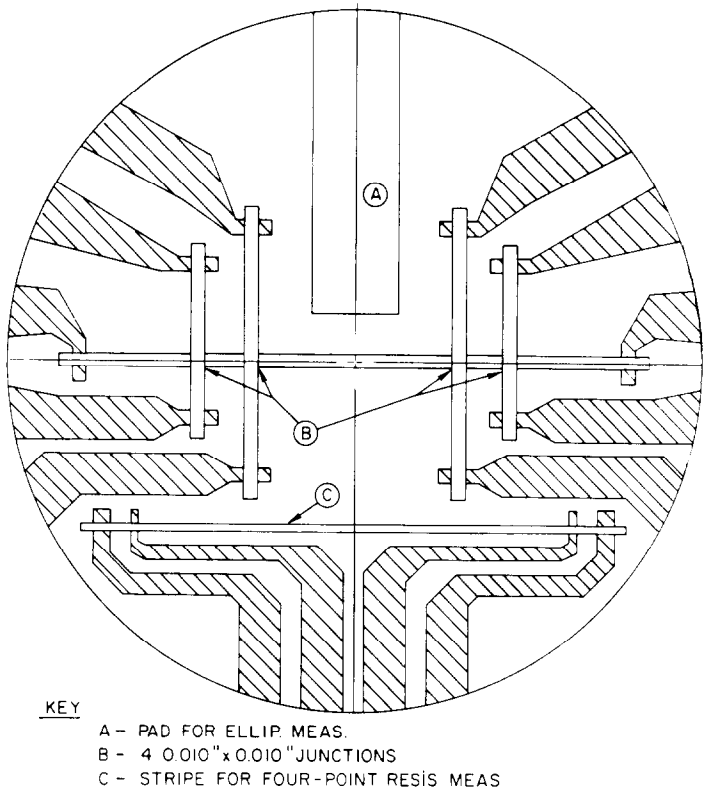

Fig. 3. Sketch of 1 in. dia. substrate with contact lands, four-point resistivity stripe and four completed tunnel junctions.

and ~ 0.001, respectively[8, 9]). When the composition of PbO is shifted towards the lead-rich side by chemically reducing heat treatments[8]), κ can approach $\sim 10^{-2}$; larger values might be anticipated for highly stressed and/or disordered films. In this situation, fig. 5 can be used to estimate X and κ, assuming $n_{PbO} = 2.8 = \text{constant}$.

Minor structural and/or compositional variations in an oxidizing metal system can be detected sometimes by computing κ versus n curves from the Δ, ψ sets for each oxidation time. Using this approach, the authors[11]) have observed systematic shifts in the n–κ curves for In_2O_3 during the room temperature oxidation of indium films. Thus κ was determined to decrease linearly as X increased for a constant $n_{In_2O_3}$ value, suggesting that such shifts arise from a gradual decrease in excess In^{+3} ion concentration as the In_2O_3 thickens.

When similar calculations were carried out for lead films oxidized near room temperature for times from several minutes to weeks, all the n–κ curves

were found to lie within the narrow envelop shown in fig. 6, indicating that the optical properties of the metal–oxide system remain unchanged under these conditions as X increases.

3.2. Lead film stability effects

Data will be presented here illustrating the influence of lead microstructure on the oxidation process. The calculated n_{Pb} and κ_{Pb} values depend on the lead surface topography and attempts have been made to compute the apparent optical constants for metals having various idealized surface configurations (e.g., regular pyramids)[12]). If the lead smoothness changes noticeably during the oxidation run, X and n_{PbO} values computed using the pre-oxidation n^*_{Pb} value can be considerably in error.

Accordingly, the lead film stabilities were established by monitoring the

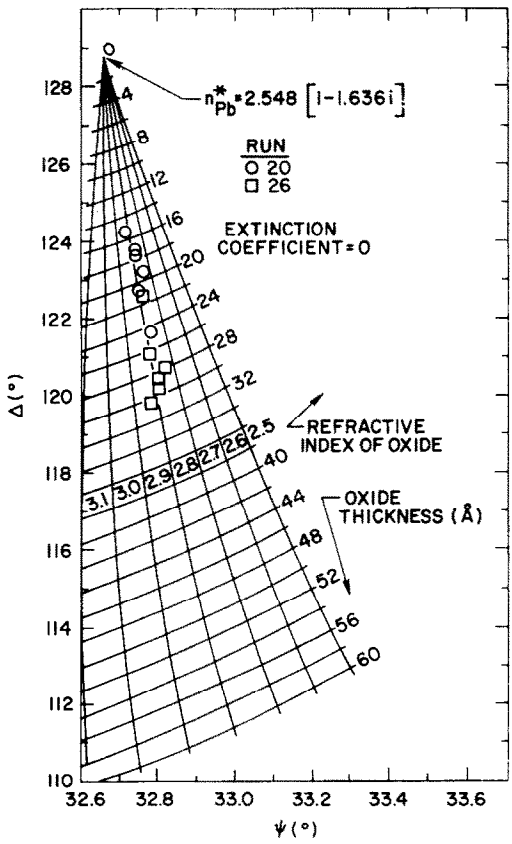

Fig. 4. Δ versus ψ results for two runs, made at 25°C and 1 atm O_2, showing that $n_{PbO} = 2.8$ for $\kappa_{PbO} = 0$.

constancy of the n^*_{Pb} value, on holding the *unoxidized* films in vacuum at temperature for times up to 2 hr before admitting oxygen. For temperatures $\lesssim 80\,^\circ C$ for 3000 Å thick polycrystalline Pb films on sapphire or $\lesssim 150\,^\circ C$ for single crystal lead on mica, significant surface restructuring occurred within this time period. Recrystallization effects on n^*_{Pb} were studied to some

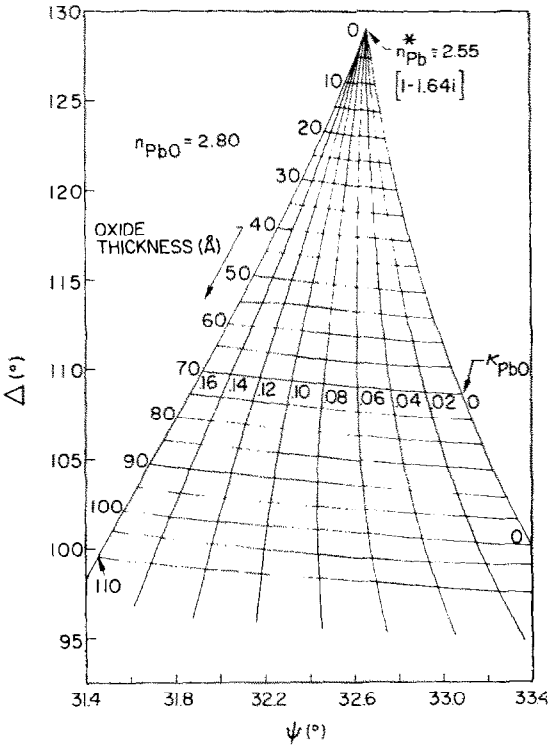

Fig. 5. Families of Δ–ψ curves for various κ-values, assuming $n_{PbO} = 2.8$.

extent at 112 °C, using 2000 to 15000 Å thick lead films. (See fig. 7). For the thinner films on sapphire, the apparent n_{Pb} and κ_{Pb} values correspond to large (4 to 8°) *decreases* in the Δ and ψ parameters from their normal values. Electron microscopy revealed that the surfaces of these specimens had large, flat-bottomed pits ($\sim$1000 to 2000 Å deep) while films with essentially normal optical constants were quite smooth. The films on mica exhibited greater resistance to recrystallization, probably because of the absence of grain boundaries and the stronger mica–lead adhesive forces relative to the sapphire–lead one.

Lead recrystallization can also accelerate the oxidation, as is evidenced by

the results in fig. 8. Note that $X^{-1} \approx \log \text{time}^*$, and the rates on sapphire increase rapidly as the lead thickness is reduced. Growth is comparitively insensitive to lead thickness when mica substrates are used under these conditions but not at $\sim 150\,^{\circ}\text{C}$ or higher.

The oxidation enhancement probably has the following origins: (1) at temperatures of $\sim 373\,^{\circ}\text{K}$ ($\approx \frac{2}{3}$ of the melting point of lead), PbO is harder

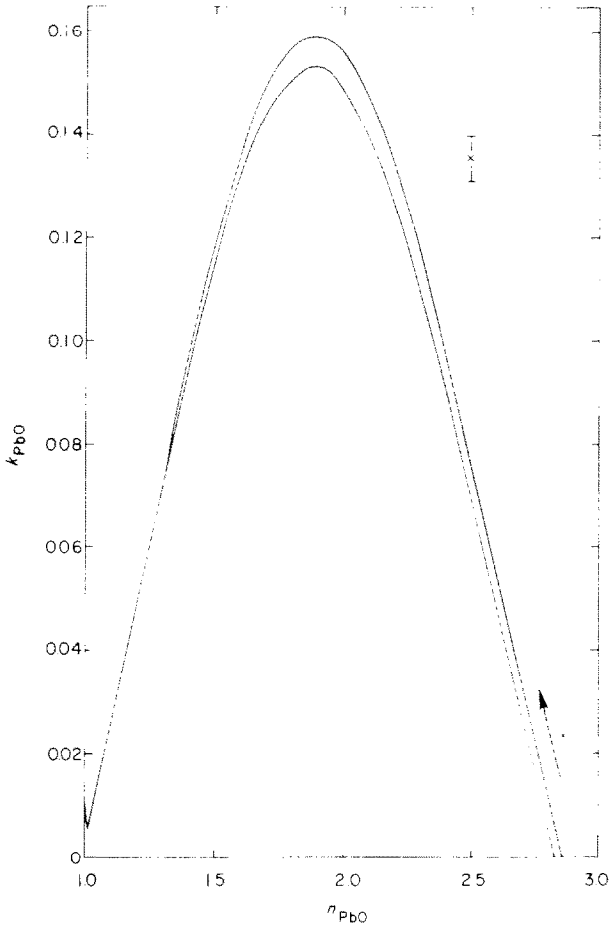

Fig. 6. κ_{PbO} versus n_{PbO} curves computed for various lead oxidation times. All curves (for times from 1 to 10000 min) fell within the indicated envelope. Maximum experimental error is indicated by the error bar.

* This inverse logarithmic dependence can be derived by an approximate integration of the growth law, $dX/dt = \alpha \exp(X_1/X)$, where α and X_1 are constants whose values depend on the reaction chemistry. Although such plots are quite satisfactory for displaying the raw X–t data, a more exact integration of the rate equation is used in Part II for analyzing the oxidation mechanism.

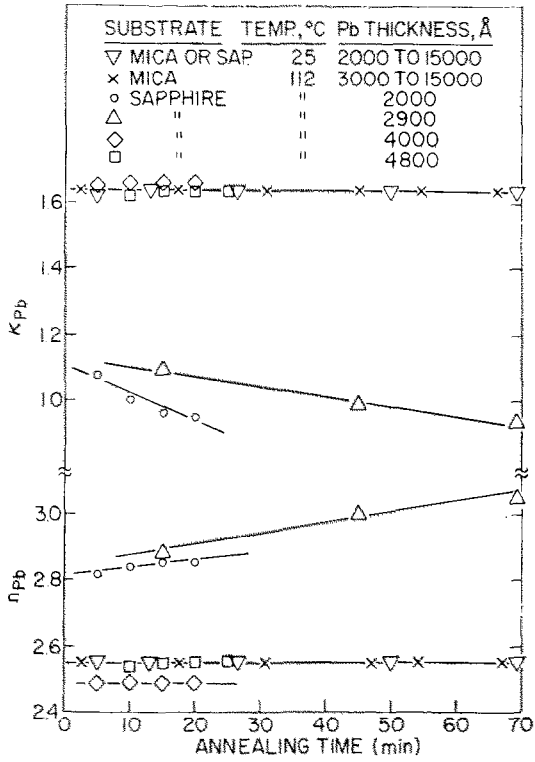

Fig. 7. Changes in the measured optical constants of various lead film–substrate systems, during vacuum annealing at 112°C.

than the Pb phase; (2) the lead is under a tensile stress in the interfacial plane, as will be apparent from the later X-ray results; (3) thicker lead films can internally relax more readily than thinner ones in order to accomodate the stress; (4) as the oxide thickens, stresses build up until the lead flows plastically; and, (5) this ruptures the protective oxide, exposing the metal to oxygen. Since the polycrystalline lead films should deform easier than the single crystal ones because of the availability of properly oriented grain boundaries, it follows that the latter type of films should oxidize slower.

Another indication the oxidation promotes roughening is provided by the relative changes in the Δ and ψ parameters. As shown in fig. 9 for a 3000 Å thick polycrystalline lead film, ψ decreases by $\sim 1°$ for a 20° decrease in Δ during oxidation at 105°C; if n_{PbO} and n^*_{Pb} were actually remaining constant, then ψ would increase $\sim 0.1°$ for a 10° decrease in Δ, as in fig. 4.

Alternately, the behavior in fig. 9 could be attributed to an oxide compositional change so that $\kappa_{PbO} \neq 0$. (Recall fig. 5.) We tend to rule out this

explanation because the ψ-parameter does not change during treatments known to be capable of chemically reducing thicker PbO layers (e.g., holding several days in vacuum at 100–200 °C)[8,9]). Under such conditions, additional stoichiometric PbO should be converted to lead-rich oxide with a further decrease in ψ. In addition, κ_{PbO} values that are approximately an order of magnitude larger than those reported[8]) for metal-rich PbO are obtained

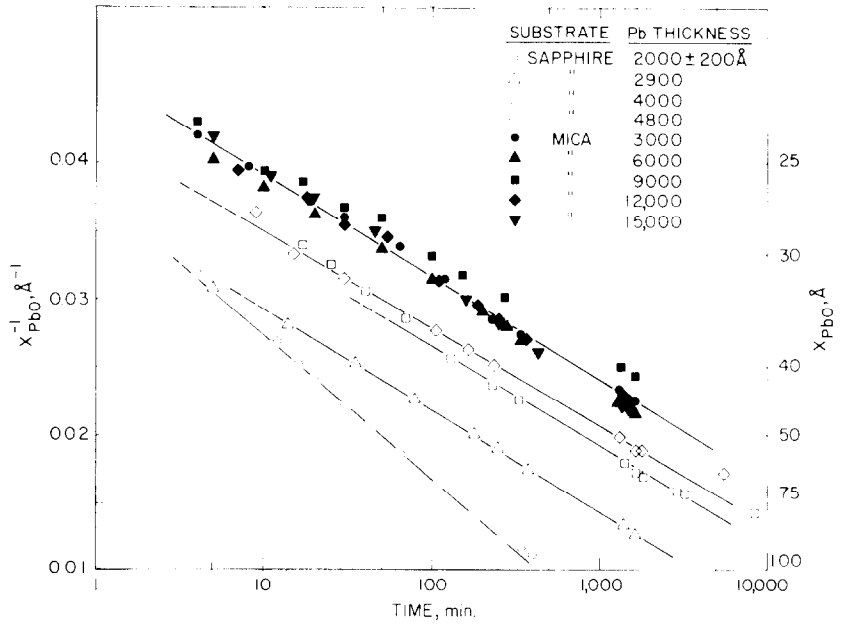

Fig. 8. Effects of lead thickness and substrate materials on the growth of PbO films at 112 °C, 1 atm O_2.

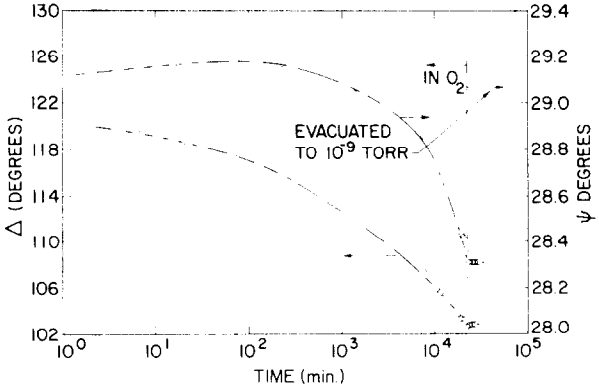

Fig. 9. Relative changes of Δ and ψ parameters when the lead surface topography is unstable (3000 Å Pb on sapphire at 105 °C).

by assuming that n^*_{Pb} is a constant when computing n–κ curves for the oxide from the data in fig. 9. (Compare figs. 6 and 10). Assuming that the behavior shown in figs. 9 and 10 arises from a changing value of n^*_{Pb}, we estimate that the computed thicknesses (based on $n=2.8$, $\kappa=0$) can be as much as 10% less than the actual values. By comparison, if the n–κ curves are very stable, then the X values are probably within 1% of the true ones.

3.3. Temperature and O_2 pressure effects

The oxidation kinetics were investigated over a temperature range, where the lead films are stable. It is convenient to show that the lead optical constants are well-behaved in this series of experiments by plotting their $n_{Pb} \cdot \kappa_{Pb}$ product against temperature. See fig. 11, and note that this product for single crystal films is ~1% greater than that for the polycrystalline layers, and is also somewhat more reproducible.

The index (for $\kappa_{PbO}=0$) of the oxide grown on single crystal lead tends to decrease with increasing temperature until temperatures of ~400°K are reached when n^*_{Pb} instabilities set in; at this point, the calculated values increase rapidly with oxidation time (or oxide thickness) as indicated by the direction of the arrows. The oxide index on polycrystalline lead is essentially constant with temperature until n^*_{Pb} effects become significant around 350°K.

Temperature effects on the X–t curves are shown in fig. 12. Note that the data closely fit a X^{-1} versus log time relationship over the range from −89

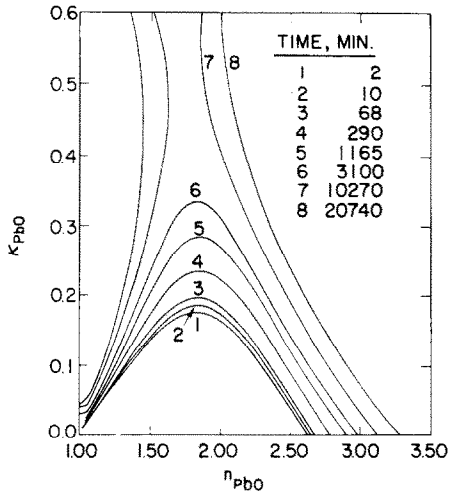

Fig. 10. κ_{PbO} versus n_{PbO} curves computed from the data in fig. 9, assuming n_{Pb}* remained constant.

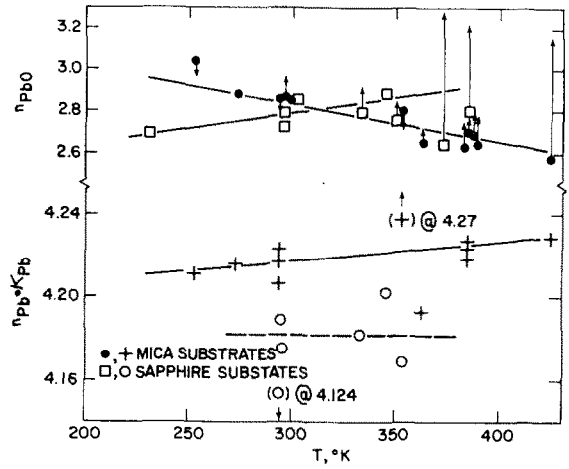

Fig. 11. Dependence of $n_{Pb} \cdot \kappa_{Pb}$ and n_{PbO} on oxidation temperature for 3000 Å Pb films at 1 atm O_2. Arrow indicates increasing time in a given run.

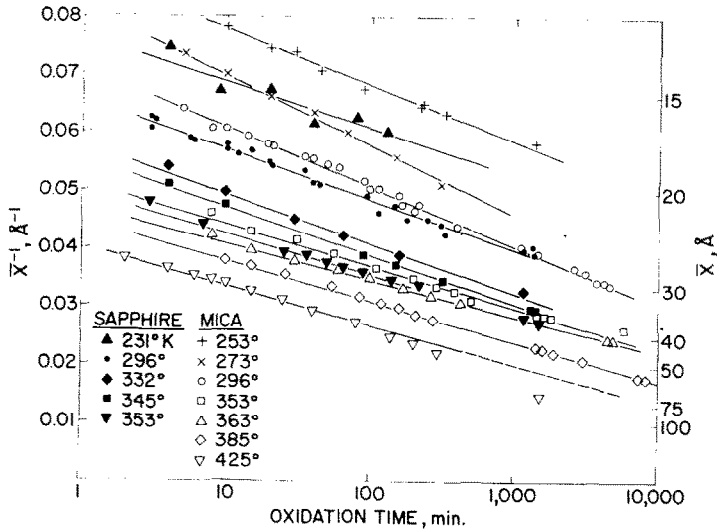

Fig. 12. Time-dependence of lead oxide growth at 1 atm O_2 and various temperatures.

up to ~150°C. For a given temperature, the polycrystalline lead oxidizes faster. The differences are small (~10%) near 23°C, but become as large as 100% at 112°C. Since there is no n–κ shift indication of surface roughening of polycrystalline films for temperatures under 80°C, the differences can be partly attributed to the presence of grain boundaries.

The room temperature–one atmosphere O_2 results compare rather poorly

with Shklyarevskii et al.[13]), who obtained: an n^*_{Pb} value of 2.24 $(1-1.88\,i)$, compared to our 2.55 $(1-1.64\,i)$; and oxide thicknesses $\sim 50\%$ larger using air ambients. Most likely, their lead films (deposited at $\sim 10^{-5}$ Torr) contained considerable amounts of oxygen since ellipsometry and Auger measurements have established that ~ 6 Å of PbO grows at this pressure in about one minute[14]). Hence, surface cleanliness differences might account for the n^* discrepancy, while their larger rates could be caused by moisture. Our limited experience indicates that traces of water accelerates lead oxidation by as much as 50%.

Another comparison can be made with the findings of Anderson and Tare[15]), who volumetrically measured the oxygen uptake at $\gtrsim 10^{-2}$ Torr O_2 on vacuum-deposited lead films. Because of the manner in which they described their results, a direct comparison of thickness–time data was difficult to make. However, their limiting thickness values (X_L, the thickness at which growth rate reaches 1 Å/day) exceeded ours by $\sim 25\%$ in the temperature range from 150 °K to 350 °K. This agreement is considered good, in view of the disparities of the techniques, experimental conditions and the assumptions involved in obtaining X_L.

The effects of pressure are shown in fig. 13, where one can see that the data again fit well to a $X^{-1} \approx \log$ time dependence and the growth rate is moderately pressure-sensitive in the 10^{-2} to 10^{+3} Torr O_2 range.

3.4. X-RAY DIFFRACTION RESULTS

In an effort to more fully understand the oxidation mechanism, several

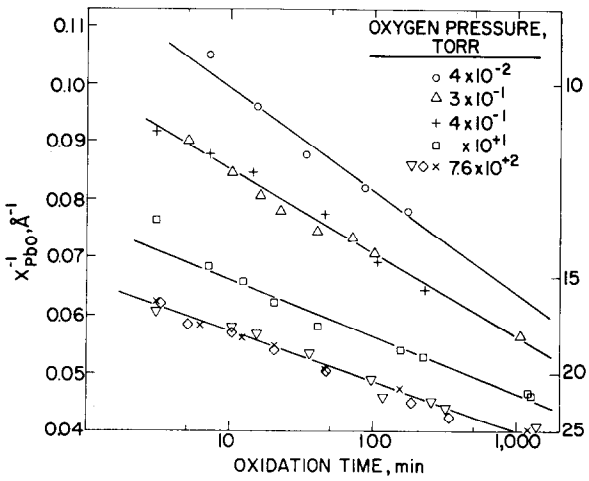

Fig. 13. Time-dependence of lead oxide growth at 25 °C and various oxygen pressures. Note the reproducibility of the 1 atm O_2 data.

specimens were studied using X-ray diffraction. While the detailed results will be published elsewhere[10]), some findings are given here. The oxide layers were found to be orthorhombic PbO (massicot) with a very strong preferred growth orientation, $(001)_{PbO} \| (111)_{Pb}$. Examination of the bulk lattice spacings suggested that the $\langle 110 \rangle$ directions of both phases were parallel; for such an epitaxial arrangement, the misfit strain was estimated to be $\sim 3.7\%$. Epitaxial forces are probably responsible for the appearance of the orthorhombic phase which is unstable below $\sim 540\,^{\circ}C$ in bulk form[16]). Such forces would not have to be large because of the small thermodynamic stability differences between the two crystalline structures, as manifested by the small enthalpy of transformation (~ 57 cal/mole) released on going to the stable tetragonal form[17]).

As shown in table 1, the ellipsometrically-determined PbO thickness are in good agreement with values estimated from the width of the (003) diffracting plane at half-peak height. This agreement would seem to be a consequence of the well-defined PbO orientation, as well as the high atomic scattering factor of lead which serves to increase the sensitivity of the method.

The large PbO strain (ε) or distension of the oxide in the z-direction indicates that large compressive forces are operative in the x–y plane since $\varepsilon_z \approx -\varepsilon_x$ (or ε_y). The average strain values were found to decrease linearly with the reciprocal of oxide thickness. Such a functional dependence has been predicted and experimentally observed for epitaxial systems where the deposited overgrowth layer is in *tension*[18]). Note also that the oxide strain is

TABLE 1

X-ray diffraction results in oxidized lead films[10])

Lead structure	PbO plane	PbO thickness (Å)		% PbO strain in z-direction**
		Ellipsometric	X-ray*	
Polycrystalline	(003)	29	38	1.7
Polycrystalline	(003)	60	64	0.495
Polycrystalline	(003)	79	77	0.25
Polycrystalline	(005)	29	–	1.5
Polycrystalline	(005)	60	–	0.65
Polycrystalline	(005)	79		0.34
Single crystal	(005)	47.4		0.43
Single crystal	(005)	73.1	–	0.03

* Estimated from the width of the (003) reflection peak at half height. Interference from the mica reflection peaks precluded the use of the (003) peaks on single crystal lead films for similar estimates.

** Estimated from $[(d - d_0)/d_0]_{100}$, where d is the measured lattice spacing of the indicated plane, and d_0 is the spacing for the same plane in the unstrained crystal, as reported in the ASTM Index.

larger, at a given thickness, when polycrystalline lead films are used. These $\bar{\varepsilon}$–$\bar{X}$ relationships will be used in Part II for explaining certain features of the oxidation characteristics.

3.5. Electron tunneling results

Since the tunnel current density (j) decreases exponentially with increasing oxide thickness[2,19]), its measurement serves as a sensitive indicator of the PbO thickness uniformity. While the tunneling experiments will be detailed elsewhere[20]), some results are shown in fig. 14 for demonstrating the technique and supporting our ellipsometric interpretation. The constancy of the $\log j$ versus X slope indicates that other barrier properties (height, dielectric constant, effective electron mass) are essentially constant for various PbO thicknesses in the 20 to 30 Å range. However, the PbO layers grown on single crystalline lead at 25 °C have j values $\sim 50\%$ less than polycrystalline lead, for a given *average* (or ellipsometrically-determined) thickness. It should

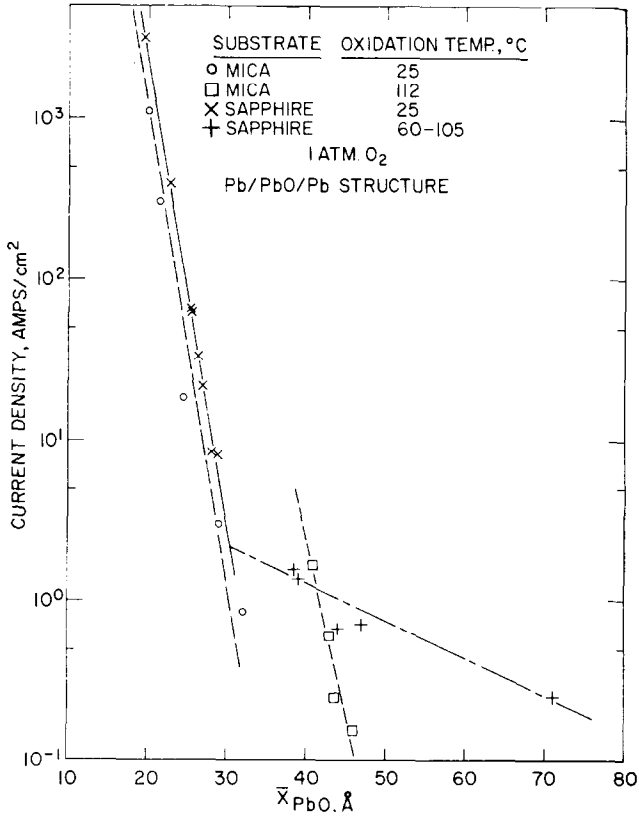

Fig. 14. Electron tunneling current density, as a function of $\bar{X}$.

be emphasized that the ellipsometric technique determines the average PbO thickness over an area of $\sim 10\ mm^2$ while tunnel currents provide a measure of the thinnest regions of the barrier which have any significant cross-section area (very roughly, on the order of several percent of the device area). In other words, even for room temperature oxidized films, fluctuations in the oxide thickness exist such that the effective tunneling distance with sapphire substrates is at least a couple of angstroms less than with mica ones. Some authors[21]) have considered the effects of barrier thickness fluctuations on properties such as current, dielectric constant, etc. by assuming various statistical distributions of thickness and relative area. At this time, there is insufficient experimental data to quantitatively confirm such models.

The effects of lead recrystallization on the thickness uniformity of PbO films grown on polycrystalline lead elevated temperatures can now be appreciated. Recall fig. 11 and related discussion. The repeated rupturing of the PbO by plastic deformation of the lead yields oxide films with thinner regions that can be several tens of angstroms less than $\bar{X}_{PbO}$. By comparison the oxide uniformity grown on single crystal lead at elevated temperatures is much higher. It was determined also that the uniformity could be considerably improved by increasing the lead thickness from the usual 3000 Å to 6000 Å for a 100 °C oxidation, using sapphire substrates. These results suggest that PbO thickness fluctuations from the mean start to become quite significant for $\bar{X}_{PbO} \gtrsim 30$ Å, when polycrystalline Pb films on sapphire are oxidized. This value is somewhat higher, for single crystal lead on mica.

4. Conclusions

(1) Using experimental conditions such that the lead film topography remains essentially constant during oxidation, it has been determined that:
(a) The lead films have reproducible refractive indices that are slightly temperature and substrate dependent. The PbO layers have a refractive index of 2.8 for $\kappa = 0$ at room temperature; this index varies with temperature and supporting substrate material.
(b) The PbO layers have the orthorhombic crystal structure and grow epitaxially with: $(111)_{Pb} \| (001)_{PbO}$; and, probably $\langle 110 \rangle_{Pb} \| \langle 110 \rangle_{PbO}$. The average strain in the $\langle 001 \rangle$ direction in the PbO decreases rapidly with increasing oxide thickness, and depends upon the lead microstructure.
(c) The PbO thickness varies inversely with log time. The rate is sensitive to temperature, oxygen pressure and lead film structure.

(2) When oxidation runs are carried out under conditions favoring lead recrystallization, the rates are accelerated and complexly dependent upon

temperature, metal thickness and microstructure. Because of its high sensitivity to surface topography, ellipsometry is ideally suited for ascertaining whether metal film restructuring processes are contributing to the oxidation process.

(3) The ellipsometric approach is well complemented by electron tunneling and X-ray diffraction measurements. Ellipsometry is especially compatible with the design and operational requirements needed to fabricate tunnel devices *in situ* on oxide barriers of known, average thicknesses.

Acknowledgements

The authors are indebted to Drs. A. Reisman and Y. J. van der Meulen for their valuable comments on the manuscript; and to P. Balk (University of Aachen), K. D. Arfman, W. J. Rose, J. P. Gilvey and F. Genovese (MIT) for the vital roles they played in the conception, design and construction of the experimental apparatus.

References

1) See for example, J. T. Wallmark and J. H. Scott, RCA Rev. **30** (1969) 335; W. Schroen, J. Appl. Phys. **39** (1968) 2671; J. H. Greiner, J. Appl. Phys. **42** (1971) 5151.
2) J. M. Eldridge and J. Matisoo, in : *Proc. 12th Intern. Conf. on Low Temperature Physics*, 1970, p. 427.
3) N. J. Chou and P. J. Tsang, Met. Trans. **2** (1971) 659.
4) For an excellent discussion of this complex topic, see O. Kubaschewski and B. E. Hopkins, *Oxidation of Metals and Alloys*, 2nd Ed. (Butterworths, London, 1962) chs. 1 and 2.
5) See for example, C. B. Duke, *Tunneling in Solids* (Academic Press, New York, 1969); J. C. Fisher and I. Giaever, J. Appl. Phys. **32** (1961) 172.
6) See for example, J. Matisoo, IEEE Trans. Mag. **5** (1969) 848, and references cited therein.
7) Computer calculations were carried out using the program of F. L. McCrackin, Natl. Bur. Std. Tech. Note 479 (1969).
8) A. E. Ennos, J. Opt. Soc. Am. **52** (1962) 261.
9) P. B. Clapham, J. Sci. Instr. **39** (1962) 596.
10) T. B. Light, J. M. Eldridge, J. M. Greiner and J. W. Matthews, to be published.
11) J. M. Eldridge, Y. J. van der Meulen and D. W. Dong, Thin Solid Films **12** (1972) 447.
12) C. A. Fenstermaker and F. L. McCrackin, in: *Recent Developments in Ellipsometry* (North-Holland, Amsterdam, 1969) p. 85.
13) I. N. Shklyareskii, L. A. Ageev, V. P. Kostyuk and L. A. Rachinskii, Soviet Phys.-Solid State **10** (1969) 2439.
14) N. J. Chou, J. M. Eldridge, R. Hammer and D. W. Dong, J. Electron. Mater. **2** (1973).
15) J. R. Anderson and V. P. Tare, J. Phys. Chem **68** (1964) 1482.
16) A. Shunk, *Constitution of Binary Alloys*, Suppl. 2 (McGraw-Hill, New York, 1969) p. 563.
17) W. B. White, F. Cachille and R. Roy, J. Am. Ceram. Soc. **44** (1961) 170.
18) See for example, J. W. Matthews and E. Klokholm, Mater. Res. Bull. **7** (1972) 213, and references cited therein.

19) J. G. Simmons, J. Appl. Phys. **34** (1963) 2581; Brit. J. Appl. Phys. **18** (1967) 269.
20) S. Basavaiah, J. M. Eldridge and J. Matisoo, submitted for publication to J. Appl. Phys.
21) See for example, K. H. Gundlach and G. Heldman, Solid State Commun. **5** (1967) 867, and references cited therein.